Polymer Chemistry

ROYAL SOCIETY OF CHEMISTRY

PAPER

View Article Online
View Journal | View Issue

Cite this: *Polym. Chem.*, 2026, **17**, 911

3D printing with biobased epoxidized formulations based on vegetable oils with dynamic polymer network properties

Matilde Porcarello,*[a] Ettore Greco,[a] Alberto Cellai,[a] Rafael Turra Alarcon,[b] Elizabeth Rossegger[c] and Marco Sangermano [a]

In this work, we developed and characterized bio-based formulations derived from functionalized vegetable oils, aiming to create sustainable resins suitable for 3D printing with dynamic polymer network (DPN) properties. Epoxidized castor oil (ECO), known for its inherent DPN behaviour due to the presence of hydroxyl groups enabling transesterification, was used as the primary component. However, its high viscosity at room temperature limits its printability. To address this, epoxidized soybean oil (ESO), a less viscous and equally bio-based alternative, was blended with ECO in varying weight ratios: 100% ECO, 100% ESO, ECO–ESO 70–30, and ECO–ESO 50–50. UV-curing characterization of the prepared formulations was performed through FTIR and photo-DSC. Their thermal and mechanical properties were investigated through DMTA and tensile tests, while rheological analyses were conducted to assess their printability. DPN behaviour was evaluated *via* stress relaxation tests in the presence of a bio-based transesterification catalyst, eugenol-based phosphate ester (EUGP). Among the blends, the ECO–ESO 70–30 formulation retained good DPN dynamics, while in the 50–50 blend, this feature decreased due to the lack of hydroxyl groups in ESO. The DPN systems demonstrated successful 3D printability and were proven to be thermally reprocessable. This work highlights the potential of renewable, plant-oil-based materials in advancing circular and sustainable additive manufacturing technologies.

Received 12th November 2025,
Accepted 28th January 2026

DOI: 10.1039/d5py01069a

rsc.li/polymers

Introduction

Environmental issues related to the excessive production and disposal of fossil-based plastics have created growing awareness and, consequently, a pressing need to transition toward sustainable, bio-based polymer systems. However, the global plastics industry remains largely dependent on petroleum-derived resources, which significantly contribute to greenhouse gas emissions and environmental pollution. Recent analyses have shown that plastics production accounts for approximately 4–6% of global oil consumption and around 3.8% of annual greenhouse gas emissions, and this share is expected to increase by 2050 if current trends continue.[1–3]

In this context, the development of renewable and degradable polymeric materials plays a central role in reducing carbon footprints and promoting a circular materials economy.[2,4,5] Research in this field has identified several promising renewable feedstocks, such as lignin,[6] chitosan, especially for hydrogel production,[7] or bio-derived organic acids, such as itaconic acid.[8] However, vegetable oils (VOs) represent one of the most versatile and abundant categories of renewable raw materials. VOs are highly attractive for polymer synthesis due to their availability, chemical versatility, and molecular structures rich in unsaturated fatty acids, which can be easily functionalized through epoxidation, acrylation, or transesterification reactions.[5,9,10] Furthermore, their large-scale production capacity and chemical diversity (*e.g.*, soybean, castor, linseed, and sunflower oils) enable scalable routes toward high-performance bio-based materials.[11,12] Among vegetable-oil-based derivatives, epoxidized vegetable oils (EVOs)—particularly epoxidized soybean oil (ESO) and epoxidized castor oil (ECO)—have gained increasing attention as renewable epoxy monomers.[13–16] After epoxidation, the oxirane rings in these oils can undergo cationic photopolymerization under UV light in the presence of photoinitiators such as iodonium or sulfonium salts, forming crosslinked networks with tunable mechanical properties.[17,18] In some cases, a photosensitizer is added to improve reactivity or increase photopolymerization rates under UV or visible light.[19] These systems

[a]*Department of Applied Science and Technology (DISAT), Politecnico di Torino, Torino 10129, Italy. E-mail: marco.sangermano@polito.it*
[b]*Universidade de São Paulo-USP, Instituto de Química de São Carlos, 13566-590 São Carlos, SP, Brazil*
[c]*Polymer Competence Center Leoben GmbH (PCCL), Sauraugasse 1, Leoben, 8700, Austria*

have been widely used in coatings and adhesives, and more recently, have been explored as photocurable formulations in additive manufacturing.[20,21] However, two major challenges remain. The first relates to the absorption spectra of common cationic photoinitiators, which often do not match the emission wavelengths of 3D printer light sources. The second is the high viscosity of epoxy monomers, which hinders their processability. Currently, pure epoxy monomers can be processed using hot lithography 3D printers, a form of vat photopolymerization that employs UV curing while maintaining elevated temperatures to reduce viscosity and enhance curing.[15] Nevertheless, Alarcon *et al.* recently demonstrated room-temperature 3D printing of epoxidized monomers using a commercial masked-SLA 3D printer (405 nm) by employing isopropyl-9*H*-thioxanthen-9-one (ITX) and curcumin as photosensitizers.[22] Another major limitation of conventional epoxy thermosets lies in their irreversible covalent crosslinking, which, while providing excellent mechanical and chemical stability, prevents recycling and reprocessing.[21,23] To address this issue, recent research has focused on introducing dynamic covalent chemistries—such as transesterification, transamination, disulfide exchange, and imine exchange—into epoxy networks, leading to the formation of dynamic polymer networks (DPNs).[24–28] These materials maintain permanent covalent crosslinks, yet under external stimuli (*e.g.*, heat), they exhibit reversible bond exchange. Among the various mechanisms, transesterification is one of the most versatile and efficient mechanisms. Upon thermal activation, ester linkages can undergo exchange with hydroxyl groups *via* nucleophilic acyl substitution, allowing network rearrangement without depolymerization. This process enables DPNs to combine the robust mechanical properties of thermosets with the recyclability and reprocessability of thermoplastics.[16,29,30] Within this framework, the present work aims to develop bio-based photocurable formulations from epoxidized castor oil (ECO) and epoxidized soybean oil (ESO) for room-temperature 3D printing. ESO was used as a reactive diluent to reduce the viscosity of ECO and ensure printability. Their reactivity was studied using isopropyl-9*H*-thioxanthen-9-one (ITX) as a photosensitizer and a cationic photoinitiator to enhance curing efficiency. Furthermore, the introduction of a bio-based transesterification catalyst (EUGP) enabled the development of dynamic polymer networks, whose stress relaxation and thermal reprocessability were systematically investigated.

Experimental

Materials

Epoxidized castor oil (ECO) was purchased from Specific Polymers (Castries, France). Epoxidized soybean oil (ESO) was obtained from HOBUM Oleochemicals GmbH (Hamburg, Germany). The photosensitizer isopropyl-9*H*-thioxanthen-9-one-ITX (mixture of 2- and 4-isomers, 97%) and ethanol were purchased from Sigma-Aldrich. The photoinitiator 4-isopropyl-4′-methyldiphenyliodonium tetrakis(pentafluorophenyl)borate – Rhodorsil 2074 (98%) – was obtained from Rhodia. Eugenol phosphate (EUGP) was synthesized on purpose as previously reported[31] and was kindly provided by Polymer Competence Center Leoben GmbH – PCCL. The structures of the main components used in this work are illustrated in Fig. 1.

Design of formulations

In this work, formulations containing different wt% of ECO and ESO epoxy monomers were prepared. The first formulation investigated was the one with pristine ECO. Then, to lower the viscosity of this monomer, 30 and 50 wt% of ESO were added, producing ECO–ESO 70–30 and ECO–ESO 50–50 formulations, respectively. The last formulation was prepared with pristine ESO. In each formulation, 2 phr (parts per hundred resin) of photoinitiator and 1 phr of ITX were added (Table 1) and sonicated for 20 minutes at 40 °C. Additionally, to study the vitrimeric properties of the prepared samples (stress relaxation and 3D printing), 15 phr of the transesterification catalyst EUGP was added to each formulation.

Characterization methods

Photopolymerization process. Fourier Transform Infrared Spectroscopy (FT-IR) was employed to monitor the crosslinking process using a Thermo Scientific Nicolet iS50 spectrometer (Thermo Fisher Scientific, Norwalk, CT, USA). Liquid formulations were applied onto a SiC substrate, forming a 12 μm-thick layer, and were irradiated with a LightCuring LC8 (Hamamatsu Photonics; a broad-spectrum UV lamp centered at 365 nm) at 1% of the total intensity. Spectra were collected

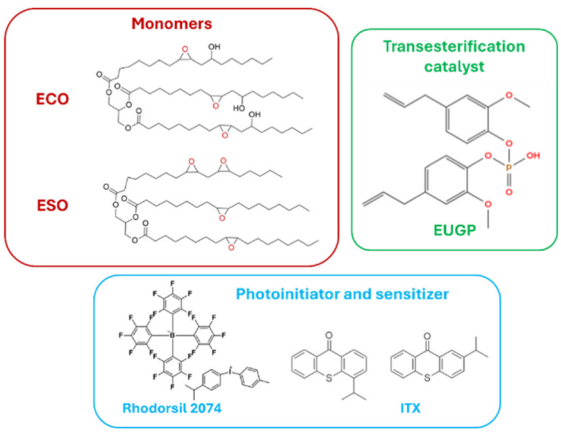

Fig. 1 Structures of the monomers, photoinitiator, photosensitizer and transesterification catalyst.

Table 1 Components for each formulation

Formulation	ECO (%)	ESO (%)	PI (phr)	ITX (phr)
ECO–ESO 100–0	100	—	2	1
ECO–ESO 70–30	70	30		
ECO–ESO 50–50	50	50		
ECO–ESO 0–100	—	100		

at a resolution of 4 cm^{-1}, and data analysis was performed using OMNIC software (Thermo Fisher Scientific). The photo-curing process was followed by observing the reduction of the epoxy group absorption band at 810 cm^{-1}, while the peak centered at 2855 cm^{-1}, attributed to the stretching of the C–H group and considered stable during the reaction, was used as an internal reference. Monomer conversion as a function of exposure time was calculated according to eqn (1).

$$\text{Conversion}\,(\%) = \frac{\left(\frac{A_{\text{fun}}}{A_{\text{ref}}}\right)_{t=0} - \left(\frac{A_{\text{fun}}}{A_{\text{ref}}}\right)_{t}}{\left(\frac{A_{\text{fun}}}{A_{\text{ref}}}\right)_{t=0}} \times 100 \quad (1)$$

where A_{fun} is the area of the functional group, in this case, the epoxy group at 810 cm^{-1}, while A_{ref} is the area of the reference group at 2855 cm^{-1}. The spectra were collected after different exposure times.

Photo-differential scanning calorimetry (photo-DSC) was also performed on the same formulations to confirm the results obtained with FT-IR. The analysis was performed with a Metler Toledo DSC-1 instrument equipped with a Gas Controller GC100. This test was performed to evaluate the rate and the heat released during the cross-linking process. For each test, 5–15 mg of liquid resin were placed in an aluminium crucible with a volume of 40 μL, while an empty crucible was used as a reference. The analysis was conducted at room temperature (25 °C), under a N_2-controlled atmosphere (40 ml min^{-1}), and for the irradiation of the samples, a Hamamatsu LC8 mercury lamp was used (Hamamatsu Photonics; a broad-spectrum UV lamp centered at 365 nm) at 10% of the intensity. The samples were subjected to a two-step cycle, each of them characterized by 2 minutes with the lamp switched off followed by 3 minutes of irradiation. The second run was performed to create the baseline and to complete the curing process. During data analysis, the second curve was subtracted from the first one to obtain a single curve related to the photo-polymerization process of the sample.

It is possible to evaluate the polymerization rate using eqn (2),[32] assuming that the heat released by the samples during the analyses originates solely from the photo-crosslinking process.

$$R_{\text{p}} = \frac{1}{\Delta H_{\text{tot}}} \cdot \left(\frac{\text{d}H}{\text{d}t}\right)_T \quad (2)$$

where R_{p} is the polymerization rate [s^{-1}], ΔH_{tot} is the enthalpy released by complete crosslinking of the sample [J g^{-1}], calculated using eqn (3),[32] and $\text{d}H/\text{d}t$ is the heat flow measured under isothermal conditions (25 °C) [J g^{-1} s^{-1}].

$$\Delta H_{\text{tot}} = n \cdot f \cdot H_{\text{ep}} \cdot \frac{1}{\text{PM}} \quad (3)$$

where n is the number of epoxy rings per mole of monomer, f is the fraction of epoxy rings that react to form the polymer network rather than participating in other reactions (in this work, $f = 1$), H_{ep} is the theoretical enthalpy for the opening of one mole of epoxy rings [J] (= −74 000 J mol^{-1} [ref. 16]), and PM is the molecular weight of the monomer [g mol^{-1}] (calculated to be approximately 975 g mol^{-1} for ECO and approximately 950 g mol^{-1} for ESO).

By integrating eqn (2), it is possible to obtain an estimate of the conversion percentage (C), according to eqn (4).[32]

$$C = \frac{1}{\Delta H_{\text{tot}}} \cdot \int_0^t \left(\frac{\text{d}H}{\text{d}t}\right)_T \quad (4)$$

For both analyses, the measurements were performed three times for each sample.

Thermo-mechanical characterization. Viscoelastic properties were investigated using a Triton Technology instrument model Tritec 2000 in tension mode. Measurements were carried out under uniaxial stress with a frequency of 1 Hz. The starting temperature of −60 °C was achieved using liquid nitrogen. Then the sample was heated at a rate of 3 °C min^{-1} until the rubbery plateau was reached. This kind of analysis was used to determine the glass transition temperature, which corresponds to the peak of the tan δ *vs.* temperature curve. DMTA was also carried out to calculate the crosslink density (ν_{c}) using eqn (5):

$$\nu_{\text{c}} = \frac{E'}{3RT} \quad (5)$$

where ν_{c} is the number of crosslinks per unit volume of the crosslinked network, E' is the storage modulus in the rubbery plateau registered at temperature $T = T_g + 50$ °C, expressed in Kelvin, and R is the gas constant. The samples used in this analysis were prepared by casting the formulations in a mold (average dimensions: 0.5 × 3.5 × 13 mm), and then they were cured using a DYMAX ECE Flood lamp (Dymax Europe GmbH) at a light intensity of 130 mW cm^{-2} for 60 s.

Printability tests. Rheological measurements were performed to establish the printability of the prepared formulations with an MCR 302e rheometer from Anton Paar (Graz, Austria), using a parallel-plate geometry (25 mm diameter of the plates). For viscosity tests, the separation gap between the plates was 0.3 mm, and the shear frequency was kept constant at 1 Hz. With this analysis, viscosity values were estimated in a range of shear rates between 0.1 and 1000 s^{-1}. Then, the obtained viscosity values were compared to the theoretical ones for DLP/SLA 3D printing found in the literature, which are in a range between 0.2–10 Pa s and 5–20 s^{-1} [ref. 13].

In addition, depth-of-cure measurements were also performed to optimize printing parameters. Cure-depth measurements were performed directly on the vat of the printer (Phrozen Sonic Mighty 4 K, 405 nm) without the platform. A certain quantity of slurry was deposited at the centre of the vat, and it was exposed to different irradiation times. Subsequently, the cured samples (square shaped 25 × 25 mm^{-2}) were removed from the vat and washed several times with isopropanol and a brush was used to remove the uncured slurry. Then, the thickness of the samples was measured using a micrometer. Three measurements were taken at different locations on the sample to assess whether the thickness was

uniform. The thickness measured corresponds to the cure depth (C_d), which is correlated with other essential parameters through eqn (6):

$$C_d = D_p \ln \frac{E}{E_c} \quad (6)$$

where C_d is the cure depth measured with a micrometer at a given exposure E, D_p is the depth of penetration of the resin, and E_c is the critical energy required to obtain gelation. E is determined by using eqn (7):

$$E = I \times t \quad (7)$$

where I is the intensity of the light source, which was measured and equal to 1.9 mW cm^{-2} (assumed as constant), and t is the exposure time at which the samples were irradiated. Then, cure-depth values were plotted against the corresponding energy exposure, creating the so-called Jacobs working curves.

By using the printing parameters calculated from the aforementioned analysis, we were able to 3D print daisy-shaped objects (10 mm × 10 mm × 2 mm). Each sample was washed in ethanol in an ultrasound bath for 5 minutes and then post-cured for 3 minutes by using a UV lamp (Phrozen Sonic Mighty, 405 nm).

Investigation of dynamic polymer network properties. Thermogravimetric analysis (TGA) was conducted to establish the range of temperature for stress relaxation measurements and to avoid the degradation of the material. The instrument used for the analysis was a Mettler Toledo TGA/SDTA 851e™. The tests were carried out by heating the samples in air from 30 °C to 550 °C at a linear heating rate of 10 °C min^{-1}.

Stress-relaxation tests were performed on the UV-cured samples using an Anton Paar MCR 302e rheometer. Discs with an average diameter of 25 mm and a thickness of about 1 mm were used. Each specimen was preloaded under a normal force of 1 N for 15 minutes at the selected temperature to ensure proper contact and thermal equilibration. A constant strain of 3% was then applied, and the decay of the relaxation modulus over time was recorded. Measurements were carried out at 150, 160, 170, and 180 °C.

The relaxation modulus, $G(t)$, was normalized with respect to its initial value, $G(t_0)$. The characteristic relaxation time of the dynamic polymer network was defined as the time required for the normalized modulus to drop to $1/e$ (≈37%) of its initial value, assuming an exponential decay behaviour described using eqn (8):[33]

$$G(t) = G_{t0} e^{-\frac{t}{\tau}} \quad (8)$$

where τ is the relaxation time [s]. The activation energy was determined by extrapolating the Arrhenius plot, as per eqn (9).[33]

$$\ln(\tau) = \ln(\tau_0) + E_a \frac{1000}{RT} \quad (9)$$

where E_a is the activation energy [J mol^{-1}], R is the universal gas constant [J mol^{-1} K^{-1}], T is the temperature [K], and τ_0 is a pre-exponential factor. By plotting $\ln(\tau)$ *vs.* $1000/T$, it is possible to calculate E_a using eqn (10), considering the slope of the curve (a):[33]

$$E_a = a \times 1000 \times R \quad (10)$$

Thermal reprocessing. Thermal reprocessing was performed to demonstrate the recyclability of these materials. Tests were performed on stress relaxation samples (with the transesterification catalyst inside) that were ground into fine pieces and placed in a dog-bone-shaped silicone mold. The mold was placed between two metal plates with a weight of 10 kg on top to apply the pressure necessary for the healing process. This system was positioned inside an oven at 150 °C for 3 hours. A similar mechanism was adopted to demonstrate the healing process on a printed sample. A flower measuring 10 × 10 mm with a thickness of 0.5 mm was printed with formulation ECO–ESO 70–30 with the catalyst that was cut in half with a blade. Then, the two halves were placed on a heated plate at 150 °C for 4 hours between two metal plates and a small weight on top.

Results and discussion

UV curing process and thermo-mechanical characterization

Photocurable formulations were initially characterized by FT-IR analysis, where the spectra were recorded at different irradiation times up to 180 seconds. As an example, in Fig. 2, the ECO–ESO 50–50 FTIR formulation is reported before and during irradiation.

Conversion and photopolymerization rates for all the investigated epoxy formulations are presented in Fig. 3. In Table 2, average conversion values with standard deviation and maximum polymerization rate values are shown.

From the data reported in Table 2 and in Fig. 3, it is possible to observe the epoxy group conversion enhancement upon increasing the weight percentage of ESO in the photocurable formulation. This can be explained by a reduction in viscosity of the formulation when ESO is added. This can lead to a higher mobility of the polymeric chains that can interact more easily with the carbocationic growing chain during the curing process. Regarding the rate of polymerization, it is possible to note that the rate is higher in the formulations containing ESO until 10 s of irradiation. Then, all the curves are overlapped, probably due to an increase in viscosity during the photopolymerization process, lowering the mobility of the chains.

To confirm this trend, photo-DSC measurements were also performed and are shown in Fig. 4. These measurements allowed the determination of the polymerization peak time under UV light, the experimental enthalpy of the reaction, and the rate of polymerization.

In Table 3, the mean values and the corresponding standard deviations are reported, obtained by analyzing the results

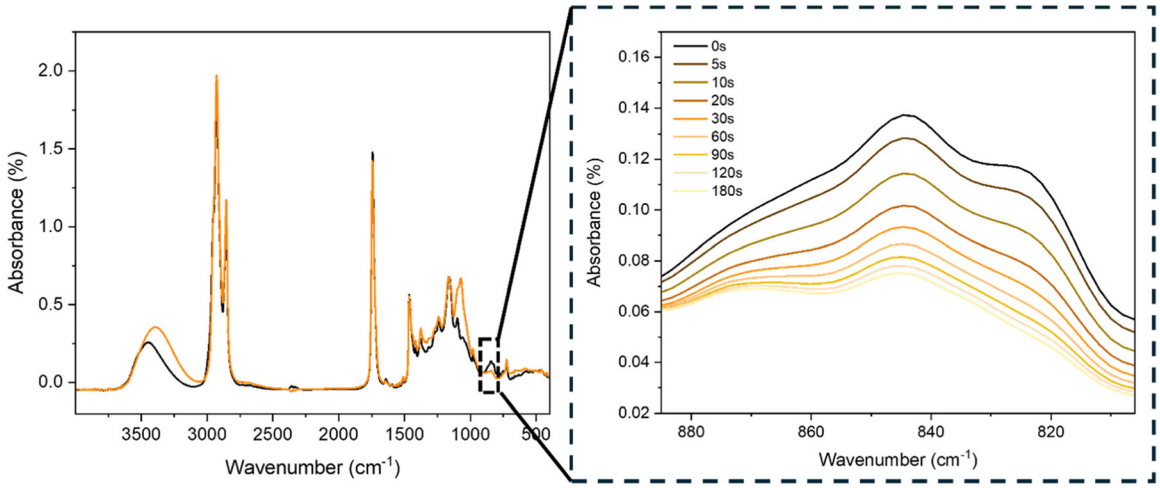

Fig. 2 FT-IR spectra of one representative formulation before and after UV irradiation with a magnification of the decreasing peak of epoxy groups.

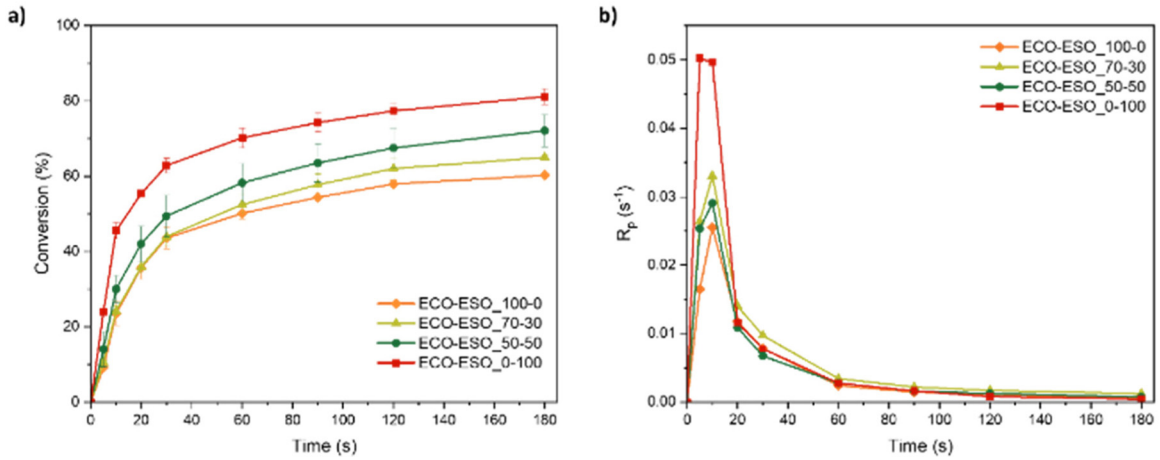

Fig. 3 Conversion curves (a) and rate of polymerization (b) curves for ECO–ESO formulations.

Table 2 Average conversion values with standard deviation and maximum polymerization rate values obtained from FT-IR analysis

Formulation	Conversion (%)	Maximum of R_p (s^{-1})
ECO–ESO 100–0	60 ± 1	0.026 ± 0.006
ECO–ESO 70–30	65 ± 1	0.033 ± 0.006
ECO–ESO 50–50	72 ± 4	0.029 ± 0.005
ECO–ESO 0–100	81 ± 2	0.050 ± 0.007

of the three measurements for each formulation, the maximum of the curves (h_{peak}), the time to reach the maximum peak (t_{peak}), and the enthalpy, calculated as the integral of the curves.

From the data reported in the previous table, it is found that the mixed formulations 70–30 and 50–50, with enthalpy values of 150 ± 9 and 139 ± 3 J g^{-1}, respectively, released greater amounts of heat during photocuring compared to the other formulations. For all formulations, the maximum peak was reached after approximately 8 s, indicating a rapid photopolymerization reaction. In addition, by using eqn (4), it was possible to calculate the conversion by considering 74 kJ mol^{-1} (ref. 16) as the theoretical enthalpy of reaction for epoxy groups. As can be observed from the conversion values, the overall trend is consistent with the FT-IR data, although the values are lower than those calculated from FT-IR. This difference can be attributed to the distinct sample thicknesses used in the two analyses. In FT-IR, the samples consist of ~12 μm-thick films, whereas in photo-DSC the samples are observed to be droplets of the formulation with a considerably greater thickness. Regarding the polymerization rate, a trend almost identical to the one observed in the FT-IR analysis was found. The maximum peak is detected by both techniques between 5 and 10 seconds, although at slightly different values. Overall, the findings from FT-IR and photo-DSC analyses are in agreement with each other.

Visco-elastic properties were investigated by means of DMTA on UV-cured films. T_g values were evaluated as the peak

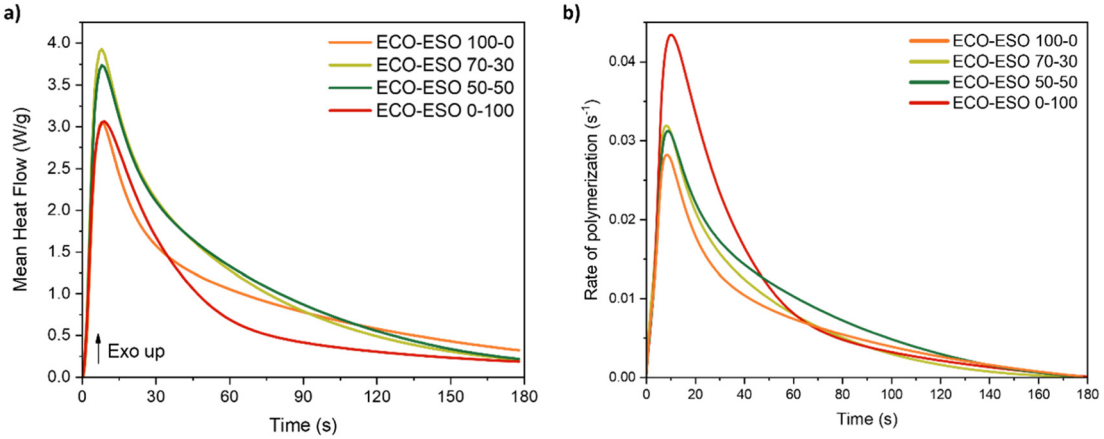

Fig. 4 Heat-flow *vs.* time curves from photo-DSC analysis (a) and rate of polymerization *vs.* time curves (b).

Table 3 Photo-DSC results regarding heat-flow *vs.* time curves, conversion calculated from this analysis and rate of polymerization

Formulation	h_{peak} (W g^{-1})	t_{peak} (s)	Enthalpy (J g^{-1})	Photo-DSC conversion (%)	Maximum rate of polymerization (s^{-1})
ECO–ESO 100–0	2.6 ± 0.9	8.0 ± 0.6	90 ± 10	41 ± 4	0.028 ± 0.006
ECO–ESO 70–30	3.7 ± 0.4	7.3 ± 0.6	150 ± 9	65 ± 3	0.031 ± 0.002
ECO–ESO 50–50	3.4 ± 0.1	7.7 ± 0.6	139 ± 3	61 ± 1	0.030 ± 0.001
ECO–ESO 0–100	2.8 ± 0.1	8.3 ± 0.6	97 ± 2	64 ± 1	0.043 ± 0.001

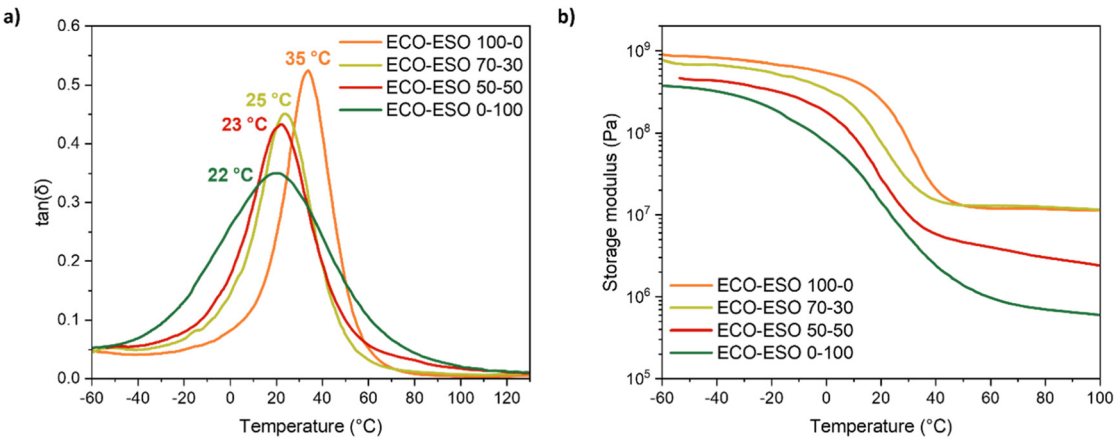

Fig. 5 Tan δ *vs.* temperature curves (a) and storage modulus *vs.* temperature curves (b) for all UV-cured formulations.

Table 4 Results of DMTA analysis and crosslink density values

Formulation	T_g (°C)	Modulus (MPa)	υ_C (mol L^{-1})
ECO–ESO 100–0	35 ± 2	11.6	1.30
ECO–ESO 70–30	25 ± 2	12.7	1.46
ECO–ESO 50–50	23 ± 1	3.3	0.39
ECO–ESO 0–100	22 ± 1	0.8	0.09

of the tan δ *vs.* temperature curve. DMTA curves for all the investigated UV-cured formulations are reported in Fig. 5.

In addition, crosslink density values were calculated with the data obtained from the DMTA exploiting eqn (5) reported in the Materials and Methods section. The results are shown in Table 4.

As shown by the data reported in Table 4, the addition of ESO led to a reduction of the crosslink density and, consequently, to a reduction in the glass transition temperature of the photocured materials due to the increased mobility of the macromolecular chains. Another factor involved in this effect is the chemical nature of the monomers: higher amounts of ECO are associated with a greater number of hydroxyl groups, which, being capable of forming hydrogen bonds, result in an increase in both the T_g and cross-link density (ν_c) while still affecting the mobility of the polymer chains.

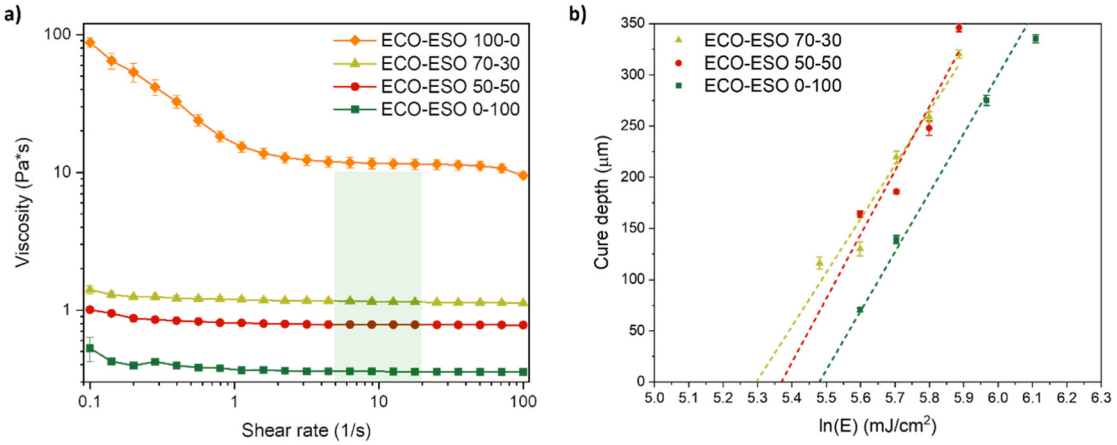

Fig. 6 Rheological behaviour with the green box representing the printability range for DLP/SLA 3D printing[12] (a) and working curves obtained with a 3D printer (b) of ECO–ESO formulations.

Determination of printing parameters

Rheological measurements at room temperature were performed to determine the viscosity of the prepared formulations to establish their printability. Viscosity *vs.* shear rate curves are reported in Fig. 6.

By examining the trend of the curves in Fig. 6, the rheological behaviour of the formulations containing ESO can be classified as Newtonian, since the viscosity remains constant over the range of applied shear stresses. In the 70–30 and 50–50 formulations, the presence of ESO acts as a plasticizing agent. These formulations also fall within the viscosity range reported in the literature as suitable for the DLP/SLA printing process, which is 0.2–10 Pa s for viscosity and 5–20 s^{-1} for shear rate.[13] Conversely, the formulation containing only ECO is not suitable for printing under these shear rate and temperature conditions. Indeed, its rheological behaviour is outside the printability range. For this reason, this formulation was not considered in the evaluation of the cure depth, which was directly performed with the 3D printer. Results of this analysis are shown in Fig. 6b. The critical energy needed to cure the resin at its gel point can be found at the intercept of the interpolating lines with the *x*-axis. The corresponding time can be found by solving eqn (7), and it was also possible to determine the amount of time necessary to obtain a 50 μm-thick layer (t_{50}), which was the decided layer thickness for the printing process. All these results are provided in Table 5.

From this analysis, it is possible to notice that as the content of ESO was increased, the formulations required longer UV irradiation times to achieve higher thickness.

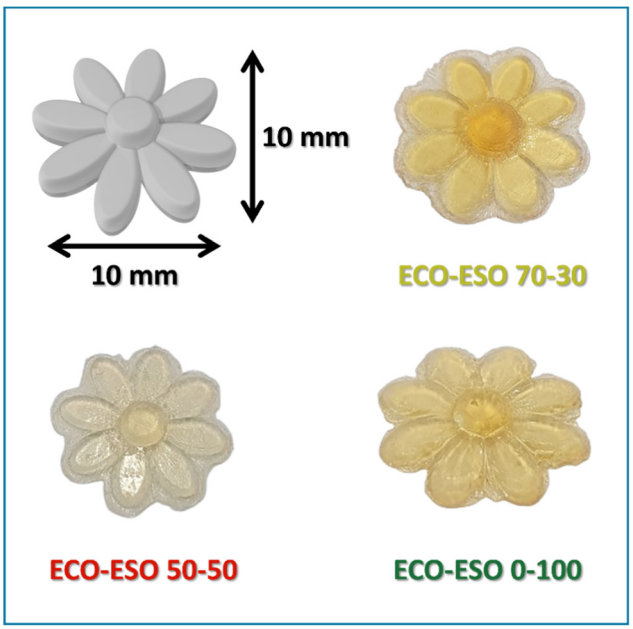

Fig. 7 Images of the CAD file of the daisy (a) and images of the 3D printed daisy with the prepared formulations: 70–30 (b), 50–50 (c), and 0–100 (d).

Higher quantities of ECO led to a faster formation of the cross-linked film that can be attributed to stronger intermolecular interactions because of the presence of hydroxyl groups involved in hydrogen bonding. This was also highlighted by the determination of the printing time. In fact, the formu-

Table 5 Cure depth measurement main results

Formulation	E_C (mJ cm^{-2})	t_0 (s)	t_{50} (s)	Irr. time for normal layers (s)	Irr. time for bottom layers (s)
ECO–ESO 70–30	200.5	67	73	90	180
ECO–ESO 50–50	213.1	71	77	90	180
ECO–ESO 0–100	240.9	80	88	100	200

lations that showed longer irradiation times are the ones containing higher quantities of ESO. The t_{50} values were used as a starting point to determine the irradiation time during the printing process. Indeed, to ensure also cross-polymerization on the *z*-axis between two following layers, we added around 10 s to each t_{50}, as shown in Table 5. For the first five bottom layers, the irradiation time was increased to enhance their attachment to the building platform. With these parameters, it

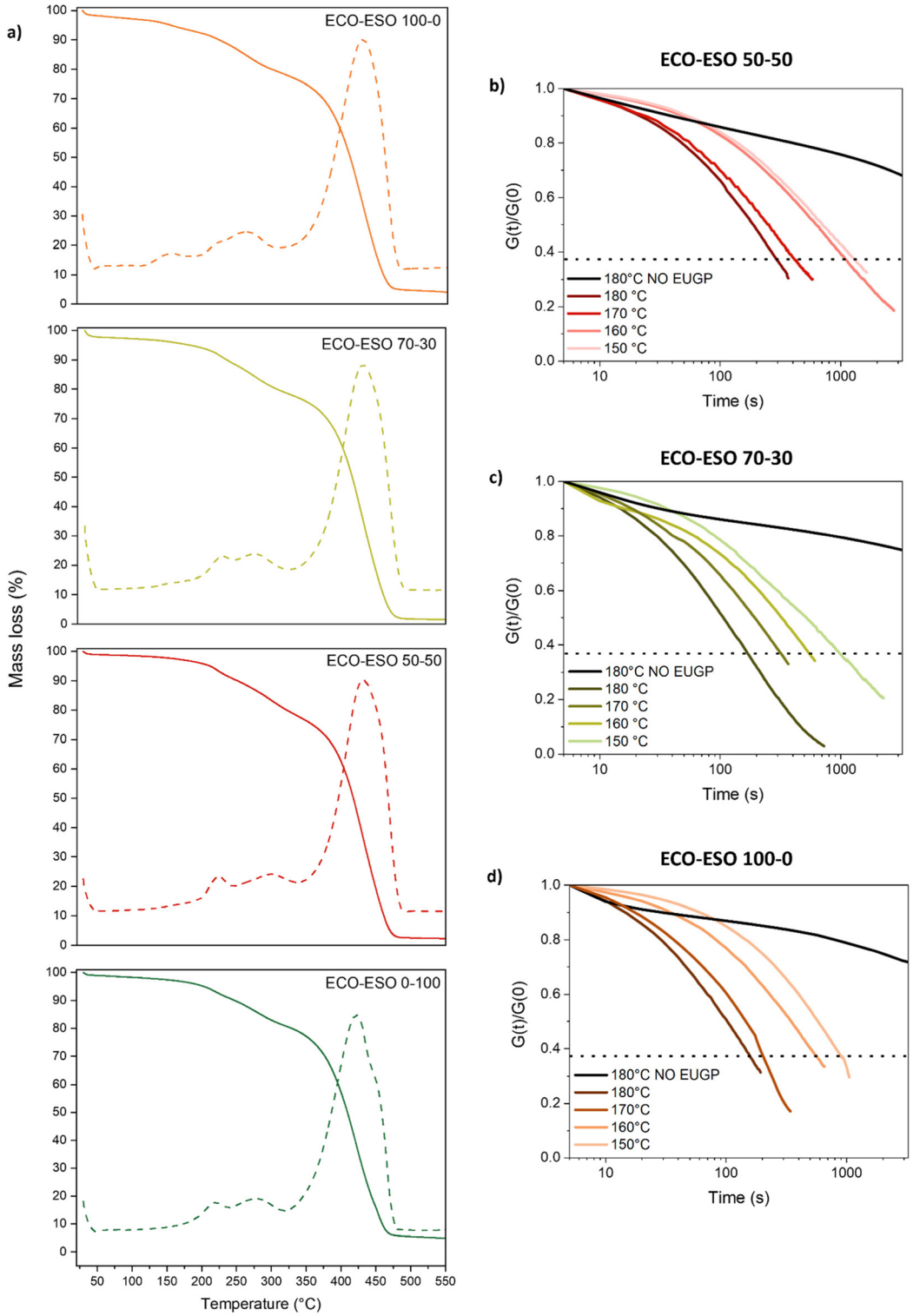

Fig. 8 TGA curves for samples prepared with ECO–ESO formulations with calculation of the first derivative represented by the dotted line (a) and stress relaxation curves for ECO–ESO 50–50 (b) ECO–ESO 70–30 (c) and ECO–ESO 100–0 (d) tested at different temperatures.

was possible to 3D print daisy-shaped objects that are shown in Fig. 7. As observed from Fig. 7, it was possible to print successfully with all the selected formulations. Overcuring is visible only in the bottom layers due to the increase in irradiation time to enhance the attachment to the platform. Overall, the 3D printing with these epoxy biobased formulations can be considered successful.

Evaluation of dynamic polymer network properties

TGA measurements were performed on UV-cured materials to establish the thermal stability of the samples prepared with the designed formulations. Results are shown in Fig. 8a. As indicated in the TGA analysis, all the formulations showed the start of the degradation process between 180 °C and 200 °C, the temperature at which the weight loss is around 5%. In the ECO–ESO 100–0 sample, a peak is visible around 150 °C, but it could be due to the presence of some humidity. Considering this, the temperatures chosen for the stress relaxation tests were 150 °C, 160 °C, 170 °C, and 180 °C, since thermal degradation did not occur at these temperatures. Then stress relaxation measurements were performed as described in the Materials and Methods section and are presented in Fig. 8b, c, and d. As expected for covalent adaptable networks controlled by associative bond-exchange reactions, all the formulations showed a gradual acceleration of the relaxation process with increasing temperature. At 180 °C, the normalized relaxation modulus of each system reached the $1/e$ threshold in the shortest time, confirming the thermally activated nature of the transesterification promoted by the biobased phosphate catalyst.

The characteristic relaxation times (τ) obtained from each curve were used to construct Arrhenius plots for the crosslinked systems (Fig. 9). In every case, the plots followed a linear trend with $R^2 > 0.97$, in line with Arrhenius-type kinetics. Increasing the ECO fraction relative to ESO clearly enhanced the rate of the dynamic exchange process. This behaviour is mainly related to the higher amount of hydroxyl (–OH) groups generated during both curing and exchange reactions of epoxidized castor oil. Owing to the coexistence of epoxy and ester groups, ECO forms secondary hydroxyls upon ring opening in the presence of the phosphate catalyst; these hydroxyls then act as nucleophiles in the transesterification mechanism responsible for network rearrangement. ESO, on the other hand, contains fewer reactive functionalities and a more aliphatic backbone, leading to a lower hydroxyl concentration after curing. As a result, ECO-rich systems possess a higher density of active sites for transesterification and therefore relax stress faster at a given temperature.

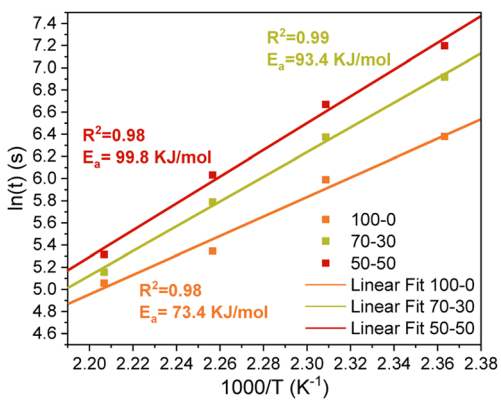

Fig. 9 Linear fitting curves calculated using the Arrhenius equation and activation energies for ECO–ESO samples.

From the Arrhenius analysis, the apparent activation energies (E_a) were calculated to be 99.8 kJ mol^{-1}, 93.4 kJ mol^{-1}, and 73.4 kJ mol^{-1} for the ECO–ESO 50–50, 70–30, and 100–0 formulations, respectively. The progressive decrease in E_a with increasing ECO content confirms that the exchange reaction becomes more kinetically accessible as the hydroxyl density rises. The faster relaxation of the ECO-rich samples is therefore consistent with their greater availability of nucleophilic sites, which facilitates bond exchange within the network. To assess whether exchange could also occur in the absence of a catalyst, additional stress-relaxation experiments were performed at 180 °C on samples prepared without EUGP. These specimens still showed a partial decay of the relaxation modulus, demonstrating that limited rearrangement can take place even without the phosphate catalyst. However, the relaxation was much slower, confirming that efficient bond exchange is mainly driven by the EUGP-catalysed transesterification. The residual relaxation observed at high temperature is likely due to slow β-hydroxy-ester exchange reactions promoted by the hydroxyl groups formed during curing,[34] together with minor contributions from residual acid/base impurities and physical viscoelastic flow. These findings highlight the essential role of the biobased phosphate catalyst in enabling rapid and thermally activated bond-exchange dynamics in the vitrimeric network.

Since the samples containing ECO showed dynamic polymer network properties, we performed thermal reprocessing on stress relaxation disks to demonstrate their self-healing capabilities. The samples were ground into fine pieces and placed inside a dog-bone-shaped silicone mold. Then, to ensure bonding between the pieces, the mold was placed between two metal plates, and a 10 kg weight was added on top. The described system was then placed inside an oven at 150 °C for 3 hours. A schematic representation of the process is illustrated in Fig. 10. As can be seen from Fig. 10, the reprocessed sample prepared with the UV-cured formulation ECO–ESO 70–30 showed self-healing ability. The same process was also successfully conducted on the sample prepared with the crosslinked formulation ECO–ESO 50–50, but at 160 °C.

A similar treatment was conducted on a printed daisy. The object was printed with the transesterification catalyst EUGP. The daisy was then cut in half with a blade and then was placed on a heated plate for 4 hours at 150 °C. To enhance the contact between the two halves, we positioned them between

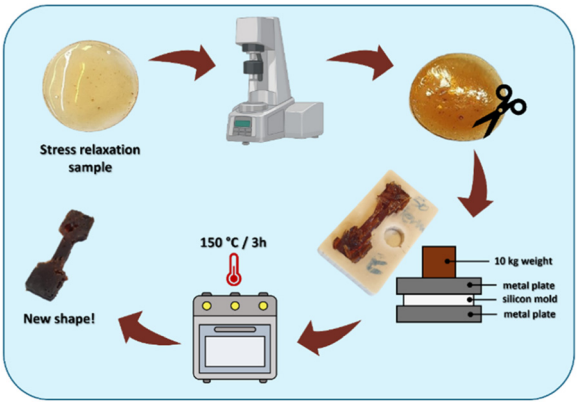

Fig. 10 Schematic of the thermal reprocessing performed on stress relaxation sample prepared with the ECO–ESO 70–30 formulation.

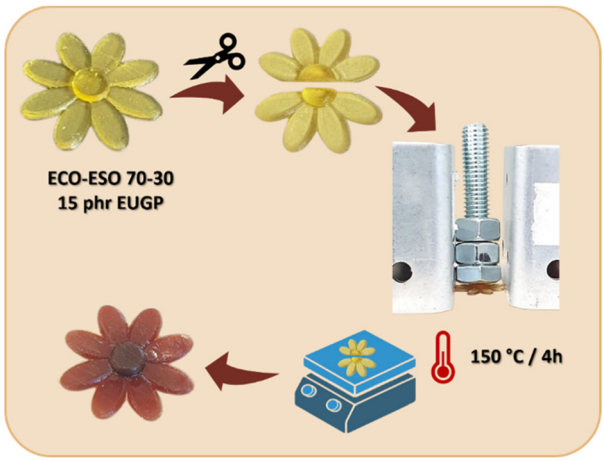

Fig. 11 Schematic of the self-healing process performed on the 3D-printed sample with ECO–ESO 70–30 with EUGP.

two metal plates with a cylindrical weight on both sides to add some pressure, and a small weight was also added on top. For a better comprehension, the scheme of the system is illustrated in Fig. 11. Also in this case, it is possible to observe the complete recovery of the initial shape. Indeed, the middle cut is not visible anymore. The same treatment was performed on the ECO–ESO 50–50 printed sample, but it was not possible to recover it to the original shape. This can be due to a lower degree of dynamic polymer network properties as shown in stress relaxation measurements and to the lower heating efficiency of the heated plate in comparison with the oven.

In addition, after all the reprocessing treatments, it was possible to see a change in the colour of the treated samples. This could be explained by a slight thermal degradation, as indicated in other studies where EUGP was used, suggesting that this catalyst could reduce the thermal stability of ester groups.[35,36]

Overall, we successfully demonstrated the self-healing capability of the designed biobased ECO–ESO formulations studied in this work.

Conclusions

This work successfully demonstrates the development of bio-based photocurable formulations prepared from epoxidized castor oil (ECO)—known for its dynamic polymer network properties—and epoxidized soybean oil (ESO), specifically designed for digital light processing (DLP) 3D printing at room temperature. This was achieved through the addition of the photosensitizer isopropylthioxanthone (ITX) in combination with the photoinitiator Rhodorsil 2074, which enabled high epoxy conversion under ambient conditions. FT-IR and photo-DSC analyses revealed that increasing the ESO content enhanced the polymerization rate due to the viscosity reduction imparted by the reactive diluent. DMTA confirmed a decrease in the glass transition temperature (T_g) with higher ESO content, attributed to greater chain mobility. Rheological and theoretical printing analyses identified optimal printability for the ECO–ESO formulations, whereas the pure ECO resin exhibited excessive viscosity, placing it outside the printable range for SLA/DLP systems. Using the printable formulations, complex daisy-shaped structures were successfully fabricated. The introduction of the bio-based transesterification catalyst EUGP imparted dynamic polymer network properties to the ECO–ESO crosslinked systems, as confirmed by stress-relaxation experiments conducted between 150 and 180 °C. Thermal reprocessing tests further demonstrated their excellent hot-press reprocessability, except for the pure ESO formulation. Moreover, samples based on the ECO–ESO 70–30 composition exhibited self-healing capability upon mild heating, confirming the dynamic bond-exchange nature of the networks. Overall, these findings establish a sustainable and recyclable platform for room-temperature 3D-printable epoxy vitrimers derived entirely from renewable vegetable oils.

Author contributions

M. P., E. G. and R. T. A. equally conducted experimental work. A. C. and E. R. performed some materials characterization. M. S. supervised the work, financed the work and corrected the paper.

Conflicts of interest

There are no conflicts to declare.

Data availability

The datasets generated and/or analysed during the current study are available from the authors on reasonable request.

Acknowledgements

This work was supported by the European Union's Horizon 2020 Research and Innovation Program under the Marie Skłodowska-Curie grant agreement, No. 101085759 (SURE-Poly).

References

1 S. T. R. Velasquez, Q. Hu, J. Kramm, V. C. Santin, C. Völker and F. R. Wurm, Plastics of the Future? An Interdisciplinary Review on Biobased and Biodegradable Polymers: Progress in Chemistry, Societal Views, and Environmental Implications, *Angew. Chem., Int. Ed.*, 2025, **64**, e202423406, DOI: 10.1002/anie.202423406.

2 S. Jha, B. Akula, H. Enyioma, M. Novak, V. Amin and H. Liang, Biodegradable Biobased Polymers: A Review of the State of the Art, Challenges, and Future Directions, *Polymers*, 2024, **16**, 2262, DOI: 10.3390/polym16162262.

3 S. Huang, Q. Dong, S. Che, R. Li and K. H. D. Tang, Bioplastics and biodegradable plastics: A review of recent advances, feasibility and cleaner production, *Sci. Total Environ.*, 2025, **969**, 178911, DOI: 10.1016/j.scitotenv.2025.178911, *Elsevier B.V.*.

4 M. Álvarez, A. Reilly, O. Suleyman and C. Griffin, A Systematic Review of Epoxidation Methods and Mechanical Properties of Sustainable Bio-Based Epoxy Resins, *Polymers*, 2025, **17**, 1956, DOI: 10.3390/polym17141956.

5 S. Ghosh and S. Ghosh, Vegetable oil-derived functional polymers in biomedical applications: hurdles and possibilities, *J. Mater. Chem. B*, 2025, **13**, 4994–5022, DOI: 10.1039/d4tb02648a, preprint.

6 L. Pezzana, E. Malmström, M. Johansson and M. Sangermano, UV-Curable Bio-Based Polymers Derived from Industrial Pulp and Paper Processes, *Polymers*, 2021, **13**, 1530, DOI: 10.3390/polym13091530.

7 R. Sesia, S. Ferraris, M. Sangermano and S. Spriano, UV-Cured Chitosan-Based Hydrogels Strengthened by Tannic Acid for the Removal of Copper Ions from Water, *Polymers*, 2022, **14**(21), 4645, DOI: 10.3390/polym14214645.

8 L. Papadopoulos, L. Pezzana, N. Malitowski, M. Sangermano, D. N. Bikiaris and T. Robert, Influence of reactive diluent composition on properties and bio-based content of itaconic acid-based additive manufacturing materials, *Discover Appl. Sci.*, 2024, **6**, 290, DOI: 10.1007/s42452-024-05926-x.

9 R. T. Alarcon, G. I. dos Santos, C. Gaglieri, A. de Moura, É. T. G. Cavalheiro and G. Bannach, Lipidic biomass as a renewable chemical building block for polymeric materials, *Chem. Commun.*, 2024, **60**, 14557–14572.

10 R. T. Alarcon, K. J. Lamb, G. Bannach and M. North, Opportunities for the Use of Brazilian Biomass to Produce Renewable Chemicals and Materials, *ChemSusChem*, 2021, **14**, 169–188, DOI: 10.1002/cssc.202001726, Wiley.

11 S. N. Khot, J. J. Lascala, E. Can, S. S. Morye, G. I. Williams, G. R. Palmese, S. H. Kusefoglu and R. P. Wool, Development and Applications of Triglyceride-Based Polymers and Composites, *J. Appl. Polym. Sci.*, 2001, **82**, 703–723.

12 C. Vazquez-Martel, L. Becker, W. V. Liebig, P. Elsner and E. Blasco, Vegetable Oils as Sustainable Inks for Additive Manufacturing: A Comparative Study, *ACS Sustainable Chem. Eng.*, 2021, **9**, 16840–16848.

13 C. Gaina, O. Ursache, V. Gaina, A. M. Serban and M. Asandulesa, Novel Bio-Based Materials: From Castor Oil to Epoxy Resins for Engineering Applications, *Materials*, 2023, **16**, 5649, DOI: 10.3390/ma16165649.

14 C. Di Mauro, S. Malburet, A. Genua, A. Graillot and A. Mija, Sustainable Series of New Epoxidized Vegetable Oil-Based Thermosets with Chemical Recycling Properties, *Biomacromolecules*, 2020, **21**, 3923–3935.

15 L. Pezzana, R. Wolff, J. Stampfl, R. Liska and M. Sangermano, High temperature vat photopolymerization 3D printing of fully bio-based composites: Green vegetable oil epoxy matrix & bio-derived filler powder, *Addit. Manuf.*, 2024, **79**, 103929, DOI: 10.1016/j.addma.2023.103929.

16 M. Bergoglio, D. Reisinger, S. Schlögl, T. Griesser and M. Sangermano, Sustainable Bio-Based UV-Cured Epoxy Vitrimer from Castor Oil, *Polymers*, 2023, **15**, 1024, DOI: 10.3390/polym15041024.

17 A. Sobhan, V. Ahirekar, M. Hoff and K. Muthukumarappan, Derivation and characterization of epoxidized soybean oil and epoxy resin film produced using a three step-washing neutralization process, *Ind. Crops Prod.*, 2023, **198**, 116675, DOI: 10.1016/j.indcrop.2023.116675.

18 W. Wang, Z. Hu and W. Lei, Research Progress on Vegetable Oil-Based UV-Curing Resins, *Polymers*, 2025, **17**(14), 1980, DOI: 10.3390/polym17141890.

19 L. Pierau, C. Elian, J. Akimoto, Y. Ito, S. Caillol and D. L. Versace, Bio-sourced monomers and cationic photopolymerization–The green combination towards eco-friendly and non-toxic materials, *Prog. Polym. Sci.*, 2022, **127**, 101517, DOI: 10.1016/j.progpolymsci.2022.101517.

20 Devansh, P. Patil and D. V. Pinjari, Oil-based epoxy and their composites: A sustainable alternative to traditional epoxy, *J. Appl. Polym. Sci.*, 2024, **141**, DOI: 10.1002/app.55560.

21 T. O. Machado, C. J. Stubbs, V. Chiaradia, M. A. Alraddadi, A. Brandolese, J. C. Worch and A. P. Dove, A renewably sourced, circular photopolymer resin for additive manufacturing, *Nature*, 2024, **629**, 1069–1074.

22 R. T. Alarcon, M. Porcarello, A. Cellai, C. C. Schmitt and M. Sangermano, Advancing green additive manufacturing: Epoxidized vegetable oils for room-temperature photopolymerization 3D printing, *Polymer*, 2025, **336**, 128868, DOI: 10.1016/j.polymer.2025.128868.

23 S. Kumar, S. K. Samal, S. Mohanty and S. K. Nayak, Electrically conductive green composites based on epoxidized linseed oil and polyaniline: An insight into electrical, thermal and mechanical properties, *Ind. Eng. Chem. Res.*, 2017, **56**, 687–698.

24 B. R. Elling and W. R. Dichtel, Reprocessable Cross-Linked Polymer Networks: Are Associative Exchange Mechanisms Desirable?, *ACS Cent. Sci.*, 2020, **6**, 1488–1496.
25 V. S. D. Voet, Closed-Loop Additive Manufacturing: Dynamic Covalent Networks in Vat Photopolymerization, *ACS Mater. Au*, 2023, **3**, 18–23, DOI: 10.1021/acsmaterialsau.2c00058.
26 W. Denissen, J. M. Winne and F. E. Du Prez, Vitrimers: permanent organic networks with glass-like fluidity, *Chem. Sci.*, 2016, **7**, 30–38, DOI: 10.1039/c5sc02223a.
27 H. Yao, X. Xu, Z. Chen, K. Li, T. Wang, S. Pei, J. Fu and J. Wang, A review of epoxy vitrimer-based thermally conductive composites, *RSC Adv.*, 2025, **15**, 37908–37925.
28 M. Caliari, F. Vidal, D. Mantione, G. Seychal, M. Campoy-Quiles, L. Irusta, M. Fernandez, X. L. de Pariza, T. Habets, N. Aramburu, J. M. Raquez, B. Grignard, A. J. Müller, C. Detrembleur and H. Sardon, Fully Recyclable Pluripotent Networks for 3D Printing Enabled by Dissociative Dynamic Bonds, *Adv. Mater.*, 2025, **37**, 2417355, DOI: 10.1002/adma.202417355.
29 C. Gaglieri, R. T. Alarcon, A. de Moura and G. Bannach, Vegetable oils as monomeric and polymeric materials: A graphical review, *Curr. Res. Green Sustainable Chem.*, 2022, **5**, 100343, DOI: 10.1016/j.crgsc.2022.100343.
30 M. Sangermano, M. Bergoglio and S. Schögl, *Biobased Vitrimeric Epoxy Networks*, John Wiley and Sons Inc, 2024, 309, 2300371, DOI: 10.1002/mame.202300371.
31 B. Sölle, U. Shaukat, E. Rossegger and S. Schlögl, Synthesis and characterization of bio-based transesterification catalysts for green 3D-printable dynamic photopolymers, *Polym. Chem.*, 2023, **14**, 4994–5003.
32 A. B. Kousaalya, B. Ayalew and S. Pilla, Photopolymerization of Acrylated Epoxidized Soybean Oil: A Photocalorimetry-Based Kinetic Study, *ACS Omega*, 2019, **4**, 21799–21808.
33 X. Liu, X. Yang, S. Wang, S. Wang, Z. Wang, S. Liu, X. Xu, H. Liu and Z. Song, Fully Bio-Based Pressure-Sensitive Adhesives with High Adhesivity Derived from Epoxidized Soybean Oil and Rosin Acid, *ACS Sustainable Chem. Eng.*, 2021, **9**, 4175–4184.
34 M. Capelot, M. M. Unterlass, F. Tournilhac and L. Leibler, Catalytic Control of the Vitrimer Glass Transition, *ACS Macro Lett.*, 2012, **1**, 789–792.
35 D. Price, L. K. Cunliffe, K. J. Bullett, T. R. Hull, G. J. Milnes, J. R. Ebdon, B. J. Hunt and P. Joseph, Thermal behaviour of covalently bonded phosphate and phosphonate flame retardant polystyrene systems, *Polym. Degrad. Stab.*, 2007, **92**, 1101–1114.
36 B. Sölle, D. Reisinger, S. Heupl, A. Jelinek, S. Schlögl and E. Rossegger, Reshapable bio-based thiol-ene vitrimers for nanoimprint lithography: Advanced covalent adaptability for tunable surface properties, *React. Funct. Polym.*, 2024, **202**, 105972, DOI: 10.1016/j.reactfunctpolym.2024.105972.